Antarctic Science 3 (4): 433–442 (1991)

On the thermohaline circulation beneath the Filchner-Ronne Ice Shelves

H.H. HELLMER[1] and D.J. OLBERS

Alfred-Wegener-Institute für Polar und Meeresforschung Columbusstraße, D-2850 Bremerhaven, Germany
[1]Present address: Lamont-Doherty Geological Observatory of Columbia University, Palisades, N.Y. 10964, USA

Abstract: In the Weddell Sea oceanographic data and numerical models demonstrate that Ice Shelf Water, one ingredient in the production of Weddell Sea Bottom Water, is formed by thermohaline interaction of High Salinity Shelf Water with the base of the Filchner-Ronne ice shelves. South of Berkner Island a passage with a water column thickness of about 300 m linking the Filchner and the Ronne regimes is important for the ventilation of the sub-ice shelf cavities. To simulate the flow we tested a two-dimensional thermohaline circulation model on several sections which approximate different geometries of a sub-ice shelf channel bounded by the ocean bottom and the ice shelf base. Temperature and salinity profiles measured in front of the Filchner-Ronne ice shelves are used to force the model. The results indicate that the circulation is sensitive to both salinity (density) forcing and depth of the shelf bottom prescribed at the open boundary representing the Ronne Ice Shelf edge. Where the shelf is shallow, 400 m deep, a closed circulation cell within the Ronne cavity acts like an ice pump with accumulation rates of marine ice at the ice shelf base up to 1.5 m y^{-1}. The total outflow at the Ronne Ice Shelf edge is supported by an inflow from the Filchner regime. Where the shelf is deeper, a flow from the Ronne into the Filchner cavity develops if the bottom salinity at the Ronne Ice Shelf edge exceeds a critical value of 34.67. Seasonal variability imposed at both edges modifies the circulation pattern at the Filchner Ice Shelf edge such that the depth and magnitude of Ice Shelf Water outflow correspond with observations in the Filchner Depression.

Received 3 September 1990, accepted 7 August 1991

Key words: Antarctica, Filchner-Ronne ice shelves, Ice Shelf Water, sub-ice shelf ocean, thermohaline circulation, numerical model.

Introduction

Interest is increasing in the role of Antarctic ice shelves in climate research. In order to calculate the state of balance of the Antarctic ice sheet and to predict its relation to global change, a better understanding is needed of the processes occurring at the ocean/ice shelf boundary, i.e. melting of ice and the accumulation of marine ice. At the base of huge ice shelves like the Ross and Filchner-Ronne (FRIS) a strong ocean/ice shelf interaction takes place according to theory (Sverdrup 1940, Doake 1976, Robin 1979), data (Jacobs *et al.* 1979, Schlosser *et al.* 1990, Jenkins & Doake 1991) and numerical models (MacAyeal 1985, Hellmer & Olbers 1989, Scheduikat & Olbers 1990). High Salinity Shelf Water (HSSW), formed by salt rejection during sea ice formation on the continental shelf is modified to Ice Shelf Water (ISW), a less saline water mass with temperatures below the sea surface freezing point. At the ice shelf edge ISW can be observed in distinct patches separated both horizontally and vertically (Carmack & Foster 1975, Jacobs *et al.* 1985, Dieckmann *et al.* 1986).

For the Weddell Sea shelf only the broad ISW plume within the Filchner Depression has been intensively investigated, although more plumes may exist toward the Antarctic Peninsula, as measurements along the ice shelf edge during the German Antarctic Expedition 1980 (Foldvik *et al.* 1985a, fig. 3) have shown. ISW can be observed on the western flank of the Filchner Depression emerging from under the Filchner Ice Shelf (FIS) and can be traced from the ice shelf edge until it flows over a sill at the shelf break. Over the continental slope it becomes one ingredient in the production of Weddell Sea Bottom Water which in turn is a component of Antarctic Bottom Water.

If the sub-ice shelf ocean were blocked by ground ice south of Berkner Island, the source of the ISW plume in the Filchner Depression could only be the small quantity of HSSW found at the base of the eastern slope (Carmack & Foster 1975, Gammelsrod & Slotsvik 1981). But to support the outflow of ISW at the shelf break, on the order of 10^6 m^3s^{-1}, Foldvik *et al.* (1985b) postulated a flow of HSSW beneath the Ronne Ice Shelf (RIS) from the shelf region toward the southern tip of Berkner Island, where a passage with a water column thickness of about 500 m exists (Pozdeyev & Kurinin 1987). A flow of opposite direction was suggested by F. Thyssen (personal communication 1988) to explain a thick layer of marine ice in the central part of the RIS. Based on these hypotheses and hydrographic section along the FRIS edge (Foldvik *et al.* 1985a) a possible flow pattern beneath the FRIS is illustrated in Fig. 1.

While the concept of southward HSSW inflow along the

east and northward outflow along the west side of the Filchner Depression is generally accepted, the paths of HSSW and ISW under the RIS are still speculative (Robin *et al.* 1983). To simulate conditions under the FRIS we have extended a two-dimensional model for the thermohaline circulation under an ice shelf (Hellmer & Olbers 1989) to include the RIS regime. For this model domain the sea floor topography is approximated along three sections, alphabetically labelled from east to west in Fig. 1. The intersections of these lines with the ice shelf edge correspond with the positions of the hydrographic stations 23, 25 and 32 (Foldvik *et al.* 1985a, fig. 3). They provide temperature and salinity profiles at the RIS edge which is one open boundary of the model. The shape of the FIS domain remains the same for all simulations. Station 292 which is situated within the inflow of HSSW under FIS in the Filchner Depression (Carmack & Foster 1975) serves as a source for the profiles prescribed at the second open boundary.

To investigate the sensitivity of the circulation to different hydrographic conditions in front of the RIS edge, the salinity profiles of stations 23 and 25 are changed. Especially for simulations along path C the salinity in the bottom layer at station 23 is varied over the range 34.65 to 34.70. Additionally a seasonal signal within an amplitude of 0.01 is imposed on the profiles of stations 23 (RIS) and 292 (FIS) to take into account the fact that exclusively summer data are available. In winter a salinity increase and temperature decrease are likely on the southern Weddell Sea Shelf due to intense cooling and sea ice formation along the ice shelf edge.

Model description

Except for the geometry of the ocean domain under the ice shelves the model is identical to the one described in Hellmer & Olbers (1989). We use the Boussinesq and hydrostatic approximations for the momentum balance, and heat and salt balances with the usual form of parameterizations for diffusion and convective adjustment as well as a nonlinear equation of state. The exchange of heat and salt with the ice shelf includes a molecular diffusive flux in the ice (for salt this is neglected), melting ice and accumulation of marine ice, and the condition of *in situ* freezing temperature at the ocean/ice shelf boundary. This dynamic and thermodynamic part of the model is supplemented by two passive tracers, ^4He and $\delta^{18}O$. The equations are applied to the sub-ice shelf cavity with the assumption that gradients parallel to the ice shelf edge (x-direction) are small. The normal flow (y-direction) is geostrophically balanced. In the y-momentum balance the Coriolis force will be neglected due to the restriction of two-dimensionality.

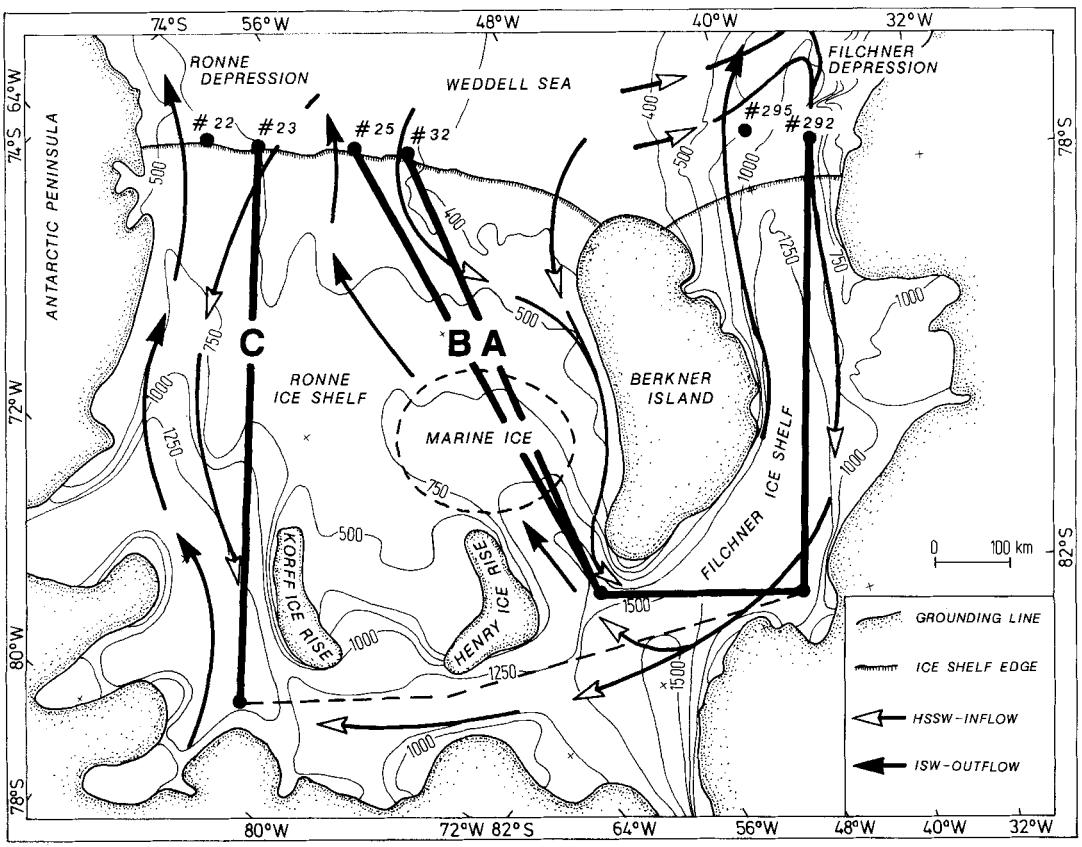

Fig. 1. Map of bottom topography beneath the Filchner-Ronne ice shelves in metres below sea level, after Pozdeyev & Kurinin (1987), including possible paths of High Salinity Shelf Water (HSSW) and Ice Shelf Water (ISW), the area of accumulated marine ice, the sections labelled with A, B and C supplying boundary conditions and the locations of stations 22, 23, 25 and 32 (German Antarctic Expedition 1980) and stations 292 and 295 (German Antarctic Expedition 1984/85).

https://doi.org/10.1017/S0954102091000524 Published online by Cambridge University Press

The vorticity equation in the y/z-plane then reads

$$\Psi_{zzt} + (v\Psi_{zz})_y + (w\Psi_{zz})_z = g\rho_y + A_H \Psi_{zzyy} + A_V \Psi_{zzzz} \qquad (1)$$

where streamfunction Ψ is defined by:

$$v = \Psi_z \text{ and } w = -\Psi_y. \qquad (2)$$

Vorticity is generated by horizontal density gradients, i.e. the flow under the ice shelf is forced by thermal and haline differences between the water in contact with the ice and the water supplied at the open edges.

In the case of a cavity which has only one open side as considered in Hellmer & Olbers (1989) the kinematic boundary condition of no flow through solid walls is satisfied by setting Ψ equal to an arbitrary constant on the boundary. For the model configuration considered here — a channel with a net through-flow under the ice shelf — we may set

$$\begin{aligned} \Psi &= 0 \qquad \text{at the bottom } z = -h_B \\ \Psi &= \gamma(t) \qquad \text{at the ice shelf base } z = -h_I \end{aligned} \qquad (3)$$

with a yet unknown function γ (t) which actually equals the total transport through the channel. This value can be determined from the requirement that any solution (1) to (3) must satisfy the momentum balance, i.e. it must ensure the existence of the pressure field p which has been eliminated in the vorticity framework. The pressure is indeed uniquely determined (Stokes' theorem) by the path integral starting from a reference point (e.g. sea surface). The integral along any arbitrary path Γ through the channel connecting the two open sides

$$\int_\Gamma \underline{\nabla} p \cdot d\underline{s} = p_2 - p_1 = \int_z^\xi g\,\rho\,dz'\,|_2 - \int_z^\xi g\,\rho\,dz'\,|_1 \qquad (4)$$

yields the difference of hydrostatic pressure, p_1 and p_2, at the side points. This difference is determined by the stratification (profiles of temperature T and salinity S) at the ice edges. In (4) $z = \xi$ is the ocean surface displacement at the ice shelf edge and

$$-\underline{\nabla} p = -(p_y, p_z) = (v_t + vv_y + wv_z - A_H v_{yy} - A_V v_{zz},\ g\rho) \qquad (5)$$

is the pressure gradient which can be calculated if the streamfunction Ψ and the density field are known.

The dynamical part of the problem given by the equations (1) to (5) is thus more complicated to solve than for the simple geometry considered in Hellmer & Olbers (1989). If treated with vorticity dynamics the problem of a channel flow is formally identical to the problem of solving for the barotropic flow in a primitive equation three-dimensional ocean model (e.g. Cox 1975) or a quasigeostrophic channel model (e.g. McWilliams 1977). Using backward time levels for advective and diffusive terms the problem reduces to the solution of two Poisson equations for the streamfunction tendencies; one with homogeneous boundary conditions and interior terms according to (1) and a second with inhomogeneous boundary conditions and zero interior terms.

The model equations are solved numerically by a finite difference scheme with forward differences in time and centred differences in space. They are integrated for ten years to reach a stationary state. The variables are placed in space on a staggered grid as described by Hellmer & Olbers (1989), where the increments Δy and Δz are constant over the entire model domain.

In addition to the kinematic boundary conditions (3) we use no-slip conditions on the solid and zero horizontal gradients at the open boundaries, i.e. $\partial/\partial/y = 0$. On the open boundaries variations in potential temperature, salinity and tracer profiles occur only in the outflow region. Wherever we have inflow the values from the measured profiles at the ice shelf edges are prescribed.

The model starts with an ocean at rest, i.e. v,w (t=0) = 0. Beneath the ice shelf the initial values for temperature and salinity are derived from the open boundary data. The ^{4}He and δ^{18}O values are initially constant over the entire model domain with 4.5×10^{-11} m^3 kgH_2O^{-1} and -0.6 $^0/_{00}$, respectively (Schlosser *et al.* 1990). They are changed by mixing with glacial meltwater which has a ^{4}He concentration of 5.6×10^{-10} m^3 kgH_2O^{-1}, calculated from Schlosser (1986) and Schlosser *et al.* (1987; station 225), and exhibits a depletion in δ^{18}O of~-42 $^0/_{00}$ (Grootes & Stuiver 1983). The air temperature at the ice shelf surface is constant and fixed at -25°C according to Jenkins & Doake (1991).

Model configuration

Approximating the data for ice shelf thickness and sea floor topography for the FRIS regime (Pozdeyev & Kurinin 1987) the model configuration is chosen such that:

a) two open boundaries exist, one at the Ronne (y = 0) and the other at the Filchner Ice Shelf edge (y = 1500 km)

b) for the FIS region the sea floor has a constant depth of z = -1200 m, whereas for the RIS region bottom topography is approximated along lines A to C (see Fig. 1) with a shelf 400 m or 500 m deep at the ice shelf edge

c) a passage with a water column thickness of 300 m connects both regimes south of Berkner Island and

d) ice shelf bases have a constant slope of 1:1000 with a depth of z = -900 m in the central part of the model domain, -200 m at the RIS and -300 m at the FIS edge.

These idealized model domains are illustrated in several of the following figures presenting two-dimensional distributions of modelled sub-ice shelf quantities.

The dynamics and thickness of the ice shelf are assumed to be time invariant. In this circumstance, no adjustments to the model domains are made to account for the melting of ice

https://doi.org/10.1017/S0954102091000524 Published online by Cambridge University Press

and the accumulation of marine ice at the ice shelf base.

Results

Due to the sparseness of data on the southern shelf of the Weddell Sea it is difficult to verify the value in this part of the model outflow region. Temperature and salinity of the modelled ISW are thus compared with general characteristics observed at other locations, and ^{4}He and δ^{18}O values with available observations from the Filchner Depression (Schlosser *et al.* 1990).

Path A (station 292 — station 32)

Depth at the RIS edge: 400 m
Salinity at the bottom on station 32: 34.65
Figs. 2,3, & 4

The structure of the flow (Fig. 2) will be discussed in connection with the potential temperature field Q (Fig. 3) and the distribution of melting/accumulation rates along the ice shelf bases (Fig. 4).

The FIS region (left side) is dominated by one circulation cell with counter-clockwise orientation. It transports relatively warm salty shelf water near the bottom into the sub-ice shelf cavity. The flow diverges where FRIS reaches maximum thickness, corresponding with the southern tip of Berkner Island. One quarter penetrates into the RIS region to support the circulation there. The major flow turns back and ascends close to the ice shelf base till it arrives at the ice shelf edge. The first contact with the ice shelf corresponds to the maximum melting rate of ~3.5 m y^{-1} in Fig. 4. This rate decreases to zero where the melt water plume is cooled down to the *in situ* freezing point. Further pressure reduction as the plume rises drops its temperature below the *in situ* freezing temperature, making it supercooled *in situ*. This thermodynamic non-equilibrium is compensated by the formation of ice crystals within the water column. These buoyant ice crystals rise to the ice shelf base, leading to the accumulation of marine ice which reaches a maximum rate of 1 m y^{-1} near the FIS edge.

Under RIS (right side) the circulation is quite different (Fig. 2). At the ice shelf edge an inflow of shelf water is absent. The whole water column is occupied by the outflow of meltwater which is supported by a flow from the FIS regime. The closed streamlines indicate that a water parcel may circulate clockwise several times within the RIS cavity before it leaves as ISW. This cell is comparable to an ice pump, driven by the change of freezing point with pressure (Lewis & Perkin 1986), which transports ice from deeper to

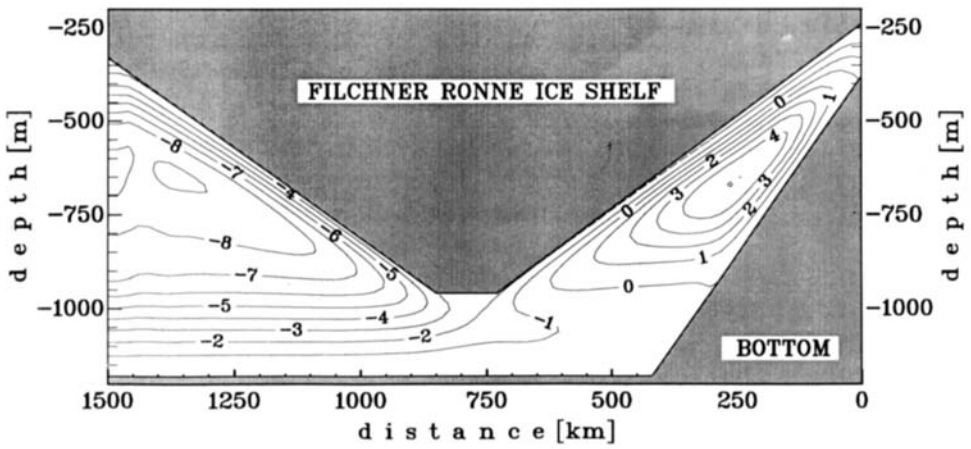

Fig. 2. Structure of flow beneath Ronne (right side) and Filchner Ice Shelves (left side) for the path A-simulation after ten years of integration. The narrow passage (central model domain) represents the area south of Berkner Island. Contour interval (CI) = 1 m^{2}s^{-1}.

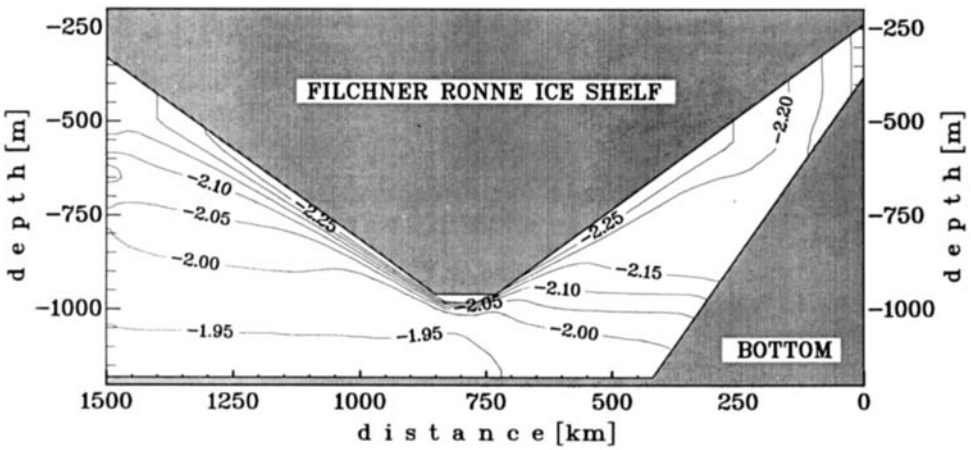

Fig. 3. Potential temperature distribution of the path A simulation after ten years of integration. CI = 0.05 °C.

https://doi.org/10.1017/S0954102091000524 Published online by Cambridge University Press

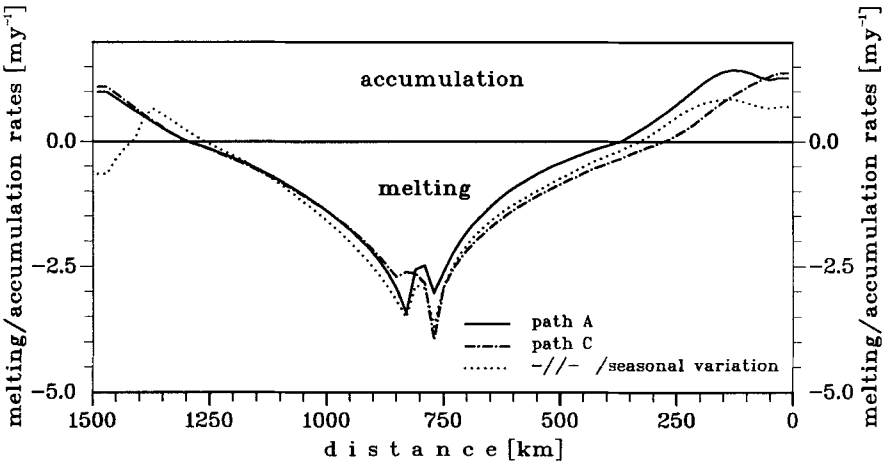

Fig. 4. Distribution of melting and accumulation rates at the Ronne (right side) and Filchner Ice Shelf bases (left side) for simulations along path A (solid line) and path C (broken line) and for the simulation with seasonal forcing at the open boundaries (dotted line).

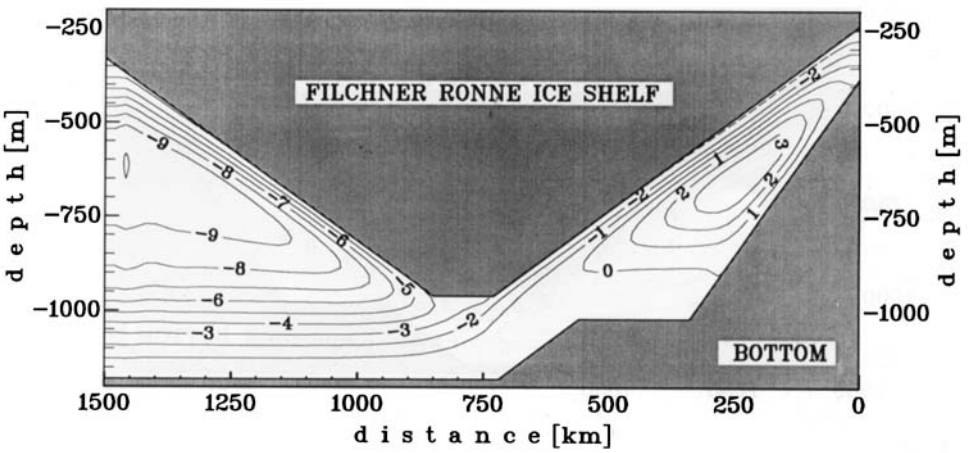

Fig. 5. Same as Fig. 2, but for the path B simulation. CI = 1 m^2s^{-1}.

higher levels of ice shelf bases. It makes the RIS cavity colder (Fig. 3), and is responsible for less melting and more accumulation (maximum rate 1.5 m y^{-1}) beneath RIS. The comparison of the modelled potential profiles at the open boundaries shows that the meltwater plume leaving RIS is slightly warmer (Θ = -2.09 °C) than that coming out from under FIS (Θ = -2.16 °C). This result agrees with observations from the FRIS edge (Foldvik *et al.* 1985a). Since both plumes separate from the ice shelf bases near their edges this temperature difference is caused by the different ice shelf drafts at both sides: this correlation was discussed by Jenkins & Doake (1991).

Path B (station 292 — station 25)

Depth at the RIS edge: 400 m
Salinity at the bottom of station 25: 34.67
Figs. 5 & 6

A comparison between Figs 5 & 2 reveals quite a similar streamline distribution along this different path. However, due to a weaker circulation cell beneath RIS the inflow from the FIS regime as well as the outflow at the RIS edge increases by 30%. As for the path A simulation the meltwater plume which occupies the whole water column prevents any HSSW inflow at the RIS edge. It becomes obvious from Fig. 6 that the first ascent of the ocean floor in the RIS region additionally hampers relatively warm (Q = -1.95 °C) and salty (S = 34.71, not shown) water of the FIS bottom layer from penetrating into the RIS cavity. The thermohaline differences between water in contact with RIS and water flowing near the bottom are smaller. This again reduces horizontal density gradients and weakens the RIS circulation cell.

Increasing the bottom salinity at the RIS edge up to 34.80, a value only observed close to the Antarctic Peninsula (Foldvik *et al.* 1985a), does not change the circulation pattern under FRIS. As no direct inflow of HSSW from the shallow shelf region exists, as in Fig. 5, initially saltier water in the RIS cavity is diluted by a higher meltwater flux. This again reduces the horizontal density gradients and consequently slows the circulation to a level at which the FIS cell transports water into the RIS regime.

Path C (station 292 — station 23)

Depth at the RIS edge: 500 m
Salinity at the bottom of station 23: 34.68
Figs. 4,7,8 & 9

As the Ronne Depression close to Antarctic Peninsula (Fig. 1) is a favourable region for an inflow of the saltiest fraction

https://doi.org/10.1017/S0954102091000524 Published online by Cambridge University Press

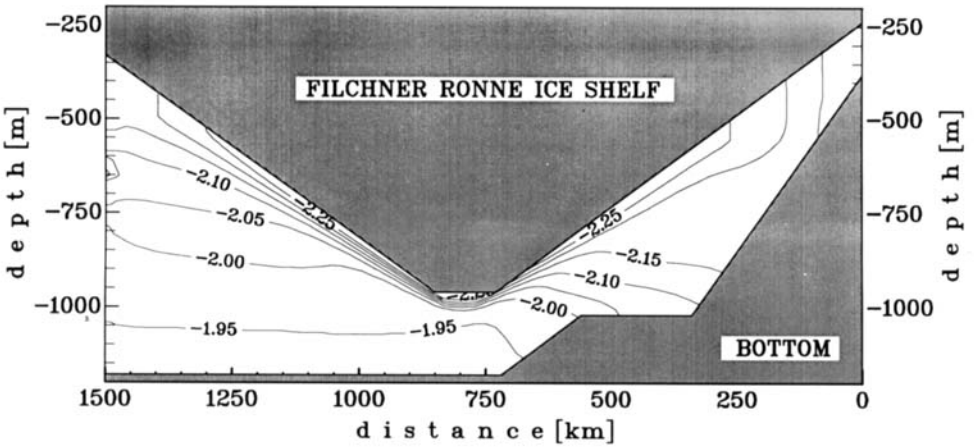

Fig. 6. Same as Fig. 3, but for the path B simulation. CI = 0.05 °C.

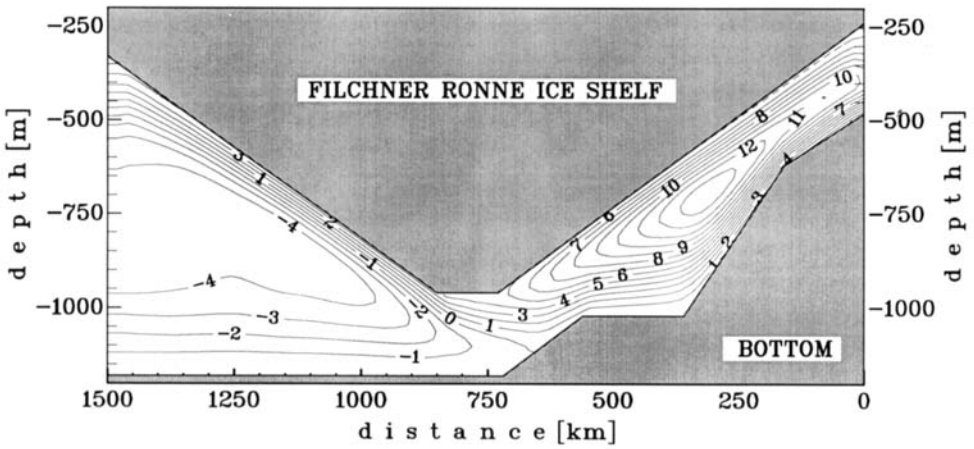

Fig. 7. Structure of flow beneath Ronne (right side) and Filchner Ice Shelves (left side) for the path C simulation with a bottom salinity of 34.68 at station 23. CI = 1 m^2s^{-1}.

of HSSW beneath RIS, a simulation along *path C* might connect the most important areas for a ventilation of the FRIS cavity. The westerly part of *path C* roughly follows the flow of Rutford Ice Stream so that our results can be compared with those of a one-dimensional plume model applied to the same region by Jenkins & Doake (1991). To avoid an elongation of our model domain, we assume that ocean/ice shelf interaction occurs only along the solid lines in Fig. 1, whereas water masses pass unmodified along the broken line.

For this simulation with a deeper shelf at the RIS edge and an initially more saline cavity a remarkable change in the circulation pattern beneath the FRIS occurs. Although both regimes are dominated by cells with the same orientation as discussed for *path A*, the strength of the FIS cell is now decreased, whereas that of the RIS is increased by a factor of four (Fig. 7). Near the bottom the latter cell transports HSSW from the RIS edge toward the interior. Where FRIS reaches maximum thickness the flow diverges to support the meltwater plumes of both regimes. Compared with previous simulations the HSSW inflow under RIS makes that sub-ice shelf cavity warmer and saltier. The thermohaline differential increases in combination with an intensification of the circulation. Consequently, higher melting occurs at the interior ends of *path C* (maximum rate 4 m y^{-1}) and smaller accumulation is simulated along the RIS base (Fig. 4).

The modelled potential temperature profiles at the FIS and RIS edges (Fig. 8) show a colder Filchner outflow. The temperature minimum (T_{min}) of the Filchner profile (solid line) is within the measured range for ISW outflow in the Filchner Depression at station 295 (dotted line). Whereas the T_{min} of the plume leaving the RIS cavity (Θ = -2.10 °C, broken line) is close to the ISW plume temperature observed by Foldvik *et al.* (1985a) at station 22 about 70 km to the west of station 23. At both FIS and RIS edges values for ^{4}He: 4.7x10^{-11} m^3 kgH_2O^{-1} and $\delta^{18}O$: -0.7 $^{o}/_{oo}$ correspond with observations in front of the FIS edge (Schlosser *et al.* 1990).

From previous simulations (Hellmer & Olbers 1989) we know that the circulation within the sub-ice shelf cavity is influenced by the salinity profile (and hence density) prescribed at the open boundary. As in the case of the *path B* simulation, hydrographic conditions in front of RIS were changed. Salinity in the bottom layer of station 23 was decreased to 34.65 while that at station 292 was maintained at 34.72. It turns out that for the *path C* version a critical inflow salinity of 34.67 exists at which two circulation cells develop, but without any flow from one regime into the other. For higher values relatively warm salty shelf water flows from the RIS cavity to the FIS (Fig. 7) supporting the ISW outflow in the Filchner Depression, whereas for lower values

https://doi.org/10.1017/S0954102091000524 Published online by Cambridge University Press

the direction of this bottom flow reverses. Using 34.65, water masses from the FIS enter a RIS cavity dominated by a weak circulation cell with clockwise orientation (Fig. 9). Any shelf water flowing directly under RIS, ascends towards the ice shelf base before the deepest part is reached. The decrease in the strength of the flow causes lower melting rates along the RIS base, while rates under the FIS are quite similar in all model runs.

Seasonal forcing at the open boundaries of path C

Figs. 4,10 & 11

During winter high sea ice production is assumed to enhance vertical salt flux by brine rejection on the southern Weddell Sea shelf (Gill 1973). Particularly in front of the ice shelves, HSSW salinity may at times exceed 34.80 as observed in the western Ronne Depression where remnants of winter convection survive into the austral summer (Foldvik *et al.* 1985a, Fig. 3).

To study the effect of seasonal changes in the characteristics of HSSW on the circulation beneath FRIS we imposed an amplitude of 0.01 on the measured salinity profiles at the open boundaries of the path C simulation. That is, in the bottom layer the salinity ranged from

34.71 to 34.73 at station 292 and
34.67 to 34.69 at station 23.

The chosen variations are small in comparison to figures that could be attributed to the enhanced sea ice production in winter. Nevertheless, after ten years of integration with a seasonal cycle for the last five years the modelled oceanographic environment is different, although the simulation ends with bottom layer salinities of 34.72 at station 292 and 34.68 at station 23.

Forced by an enhanced (~ factor 3) FIS circulation a weak transport of shelf water into the RIS cavity still exists (Fig. 10), but the major part of the flow turns back to ascend along the FIS base. After a shorter distance of ice shelf/ocean interaction the meltwater plume separates from the ice shelf base and spreads out horizontally toward the FIS edge at mid-range depth. It allows water masses from higher levels of the water column to penetrate beneath the ice shelf. This situation, comparable to the standard simulation result of Hellmer & Olbers (1989, Fig. 5), is also reflected in the modelled potential temperature profile at the FIS edge (Fig. 11, solid line). The T_{min} layer (Θ = -2.23 °C) is cooler than in Fig. 8 due to the separation of the meltwater plume at greater depth. Inflow of warmer water in the upper part causes both a strong temperature gradient (Fig. 11) and melting near the FIS edge (Fig. 4). However, the melting rate of 0.65 my^{-1} there reflects only the thermohaline portion of melting at the ice shelf edge and is still less than observed (Jenkins & Doake 1991).

The circulation under RIS is reduced by one half. Less inflow of shelf water makes the cavity colder, so that melting

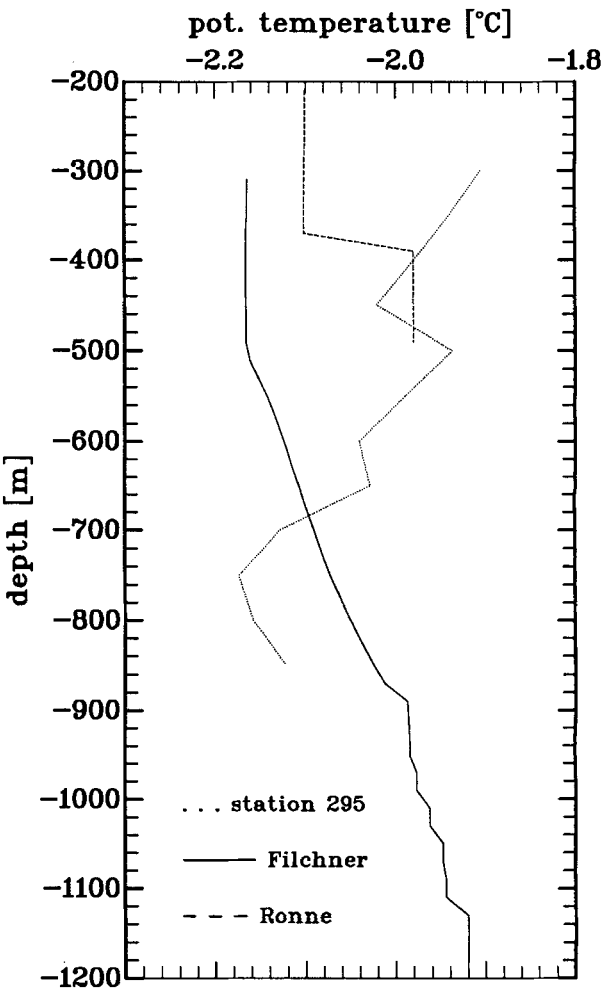

Fig. 8. For the path C simulation the comparison between modelled potential temperature profiles at the Filchner (solid line) and Ronne Ice Shelf edges (broken line) and the profile at station 295 (dotted line); location of station 295 marked in Fig. 1.

beneath RIS and consequently the density gradients decrease. The separation of the meltwater plume at ~350 m is recognisable in the potential temperature profile at the RIS edge (Fig. 11, broken line), and corresponds with the depths of the ISW core at station 22 (Foldvik *et al.* 1985a, Fig. 3). The gradient in the upper part of the profile reflects an inflow of warmer water. It reduces the accumulation rate near the ice edge to less than 1 my^{-1} (Fig. 4), but has no influence on T_{min} (Θ = -2.1°C).

A five year simulation with a salinity range of 0.04 at both stations reverses the direction of flow without qualitative changes in the variable fields. As shown in Fig. 7 a strong clockwise circulation beneath RIS transports shelf water from the ice edge into the FIS regime.

https://doi.org/10.1017/S0954102091000524 Published online by Cambridge University Press

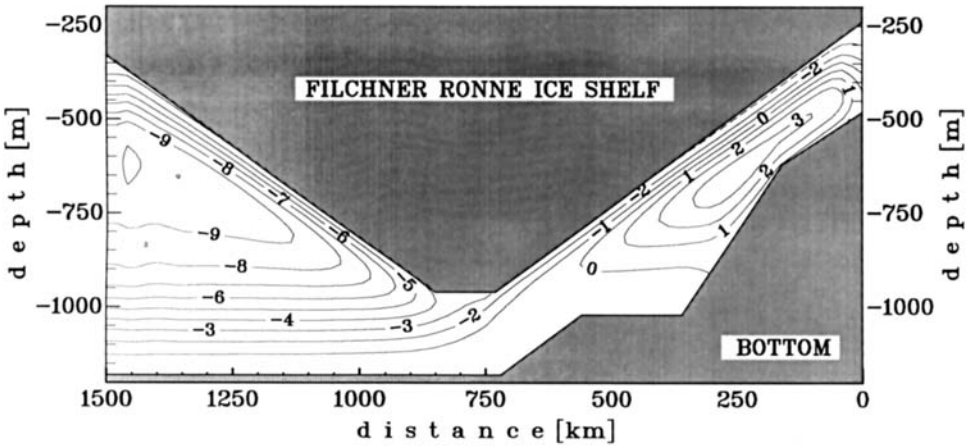

Fig. 9. Same as Fig. 7, but with a bottom salinity of 34.65 at station 23. CI = 1 m^2s^{-1}.

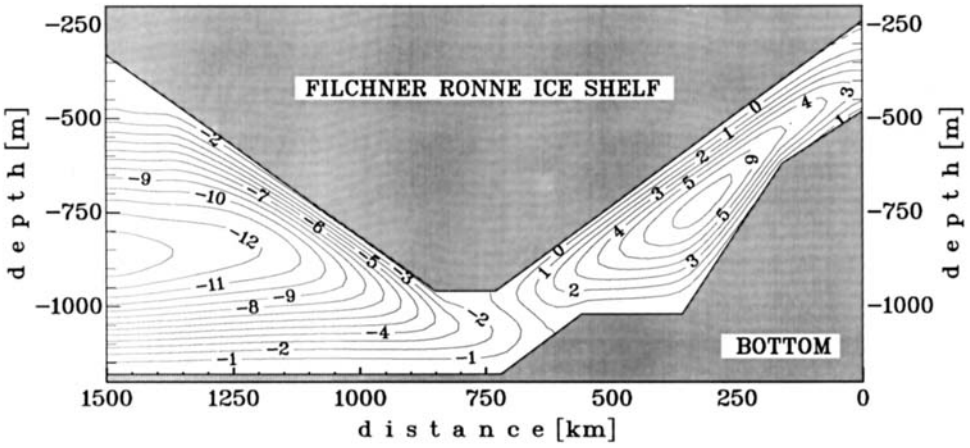

Fig. 10. Same as Fig. 7, but for seasonal forcing at the open boundaries. CI = 1 m^2s^{-1}.

Conclusions

An attempt is made to simulate the three-dimensional flow under FRIS with a two-dimensional circulation model. Data are scarce, but model results are consistent with current hypotheses about sub-ice shelf circulation. The hypotheses emphasize the importance of the area south of Berkner Island, where the direction of flow depends on both the salinity (density) profiles prescribed at the ice shelf edges and the geometry of the model domain representing the RIS regime.

One of the major difference between the results presented here and our FIS model results (Hellmer & Olbers 1989) is an increase in strength of the circulation beneath the ice shelves and higher melting/accumulation rates at their bases. The circulation is driven by a density field dominated by the exchange of heat and salt at the ocean/ice shelf boundary and again is dependent upon the intensity of inflowing salty shelf water. Linking the FIS and RIS cavities allows a more effective ventilation of the interior resulting in a stronger circulation with higher melting/accumulation rates beneath the ice shelves.

The development of a closed circulation cell under RIS depends on the depth of the shelf in front of the ice shelf and is independent of HSSW salinities (*path A* and *B*). With the accumulation rates achieved in the northern part of RIS we are able to build up the thick layer of marine ice drilled by Engelhardt & Determann (1987). Assuming an ice shelf velocity of 1000 m y^{-1} (Lange & MacAyeal 1986) and an average accumulation rate of 0.75 m y^{-1} over a distance of 350 km (Fig. 4, *path A*) a 260 m layer of marine ice accumulates at the base of RIS. This result seems to be realistic, since cooling of shelf water which enters the RIS cavity to the *in situ* freezing point can occur along an ice shelf base more than 400 km long. Accumulation of marine ice may start further southward, if an ice shelf thickness distribution with steeper slopes were used (A. Jenkins, personal communication 1990).

ISW occupying the water column between sea floor and ice shelf base has been observed at different locations in front of RIS by Foldvik *et al.* (1985a). For those regions a flow from the FIS into the RIS cavity is necessary to balance the outflow over the whole depth at the RIS edge.

For the *path C* geometry with a deeper shelf bottom (500 m) at the RIS edge the circulation is mainly influenced by the salinities prescribed at the open boundary. The critical value of S = 34.67 where the direction of flow reverses is valid only for this model configuration. However, the circulation beneath FRIS may be highly sensitive to the salinities in the Ronne Depression where the major inflow of HSSW beneath RIS is assumed.

https://doi.org/10.1017/S0954102091000524 Published online by Cambridge University Press

The RIS proportion of the *path C* results are directly comparable with those of a one-dimensional plume model for a section parallel to the Rutford Ice Stream (Jenkins & Doake 1991). In that model the derived value of the basal mass flux for the area >100 km south of the ice shelf edge, net melting of 0.65 m y^{-1}, is close to our 0.75 m y^{-1} calculated for the *path C* simulation with seasonal forcing. The location of maximum interior melting and the rate, 4 m y^{-1} near the grounding line, as well as the characteristics of the outflowing water are similar. The Jenkins & Doake (1991) plume simulated from the grounding line up to the point where it detaches from the ice shelf base is 0.1°C cooler than observed by Foldvik *et al.* (1985a), but they assume that continuous entrainment of ambient water may warm the plume on its way to the edge.

Since winter data are not yet available, seasonal variability in HSSW salinity is assumed. Nevertheless, the model results when a seasonal signal is imposed on the inflow salinities show qualitative agreement with austral summer observations in the region of outflow. Without seasonality the ISW plume does not detach from the ice shelf base; with it the outflow at the ice shelf edge varies seasonally between mid-range depth and ice shelf draft. This allows an inflow of shelf water into the upper model domain and melting near the ice shelf edge. Such changes in the flow pattern are caused by reversal or intensification of density gradients which drive the circulation, a situation comparable to the ice shelf edge oscillator discussed by Hellmer & Olbers (1989). The strength of the main circulation cell increases due to an intensification of the density gradient at the bottom. Assuming an average velocity of 0.05 m s^{-1} in the sub-ice shelf channel a salty water parcel formed during winter needs a minimum time of half a year to travel from the ice shelf edge to the central part of the cavity by which time the fresher summer component will begin to flow into the cavity.

Seasonal forcing at the ice shelf edge is responsible for an ISW outflow at mid-range depth as well as for its enhancement. On different time scales, tides may cause variable conditions near the ice edge, enhance melting in time and shifting the accumulation zone southward. If tides also force the circulation far beneath an ice shelf a higher production rate of ISW and bottom water in the Weddell Sea may be caused by stronger tides in the Weddell Sea than in the Ross Sea (A. Foldvik, personal communication 1990).

The transport of ISW out of the FIS region amounts to 1.1 x 10^6 m^3s^{-1}, if we use the value of 11 m^2s^{-1} for transport (see Fig. 10) and 1.0 x 10^5 m for the width of the ISW core on the western flank of the Filchner Depression. This outflow corresponds with the estimate of the order of 10^6 m^3s^{-1} given by Foldvik *et al.* (1985b).

We have attempted here to address some questions raised by current hypotheses regarding the ocean circulation south of Berkner Island. Numerous questions remain, such as the possibility of flow in both directions at the same time south of Berkner Island, the sensitivity of the sub-ice shelf system

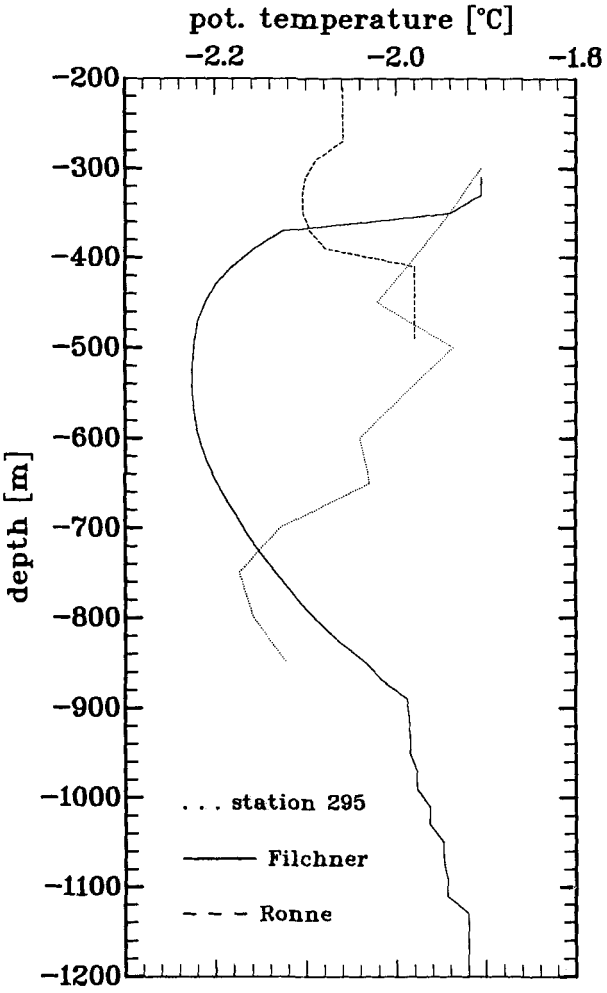

Fig. 11. Same as Fig. 8, but for seasonal forcing at the open boundaries.

to hydrographic seasonality, and the general importance of the Coriolis force, ice rises and tides for the sub-ice shelf circulation. The development of three-dimensional models and time series measurements of the oceanographic environment on the Antarctic continental shelf and beneath ice shelves should help in understanding the sub-ice shelf regimes.

Acknowledgements

We are grateful for the support of our colleagues at the Alfred-Wegener-Institute for Polar and Marine Research, Bremerhaven. A. Hense and F. Kruse gave helpful advice on model construction. S. Jacobs, E. Krenzien, A. Jenkins, J. Paren and an anonymous reviewer provided critical comments on the manuscript. The computational resources were provided by the computer centre at the Alfred-Wegener-Institute. This is contribution No. 352 of the Alfred-Wegener-Institute for Polar and Marine Research.

References

CARMACK, E.C. & FOSTER, T.D. 1975. Circulation and distribution of oceanographic properties near the Filchner Ice Shelf. *Deep-Sea Research*, **22**, 77-90.

COX, M.D. 1975. A baroclinic numerical model of the World Ocean: Preliminary results. *In Numerical models of ocean circulation*. Washington, D.C.: National Academy of Sciences, 107-120.

DIECKMANN, G., ROHARDT, G., HELLMER, H. & KIPFSTUHL, J. 1986. The occurrence of ice platelets at 250 m depth near the Filchner Ice Shelf and its significance for sea ice biology. *Deep-Sea Research*, **33**, 141-148.

DOAKE, C.S.M. 1976. Thermodynamics of the interaction between ice shelves and the sea. *Polar Record*, **18** (112), 37-41.

ENGELHARDT, H. & DETERMANN, J. 1987. Borehole evidence for a thick layer of basal ice in the central Ronne Ice Shelf. *Nature*, **327**, 318-319.

FOLDVIK, A., GAMMELSROD, T. & TORRESEN, T. 1985a. Circulation of water masses on the southern Weddell Sea shelf. *Antarctic Research Series*, **43**, 5-20.

FOLDVIK, A., GAMMELSROD, T., SLOTSVIK, N. & TORRESEN, T. 1985b. Oceanographic conditions on the Weddell Sea shelf during the German Antarctic Expedition 1979/80. *Polar Research*, **3**, 209-226.

GAMMELSROD, T. & SLOTSVIK, N. 1981. Hydrographic and current measurements in the southern Weddell Sea 1979/80. *Polarforschung*, **51**, 101-111.

GILL, A.E. 1973. Circulation and bottom water production in the Weddell Sea. *Deep-Sea Research*, **20**, 111-140.

GROOTES, P.M. & STUIVER, M. 1983. Ross Ice Shelf oxygen isotope profile at J-9. *Antarctic Journal of the United States*, **18**(5), 107-108.

HELLMER, H.H. & OLBERS, D.J. 1989. A two-dimensional model for the thermohaline circulation under an ice shelf, *Antarctic Science*, **1**, 325-336.

JACOBS, S.S., FAIRBANKS, R.G. & HORIBE, Y. 1985. Origin and evolution of water masses near the Antarctic continental margin: evidence from $H_2{}^{18}O/H_2{}^{16}O$ ratios in seawater. *Antarctic Research Series*, **43**, 59-85.

JACOBS, S.S., GORDON, A.L. & ARDAI, J.L. 1979. Circulation and melting beneath the Ross Ice Shelf. *Science*, **203**, 439-443.

JENKINS, A. & DOAKE, C.S.M. 1991. Ice-ocean interaction on Ronne Ice Shelf, Antarctica. *Journal of Geophysical Research*, **96** (C1), 791-813.

LANGE, M.A. & MACAYEAL, D.R. 1986. Numerical models of the Filchner-Ronne Ice Shelf: an assessment of reinterpreted ice thickness distributions. *Journal of Geophysical Research*, **91** (B10), 10457-10462.

LEWIS, E.L. & PERKIN, R.G. 1986. Ice pumps and their rates. *Journal of Geophysical Research*, **91** (C10), 11756-11762.

MACAYEAL, D.R. 1985. Evolution of tidally triggered meltwater plumes below ice shelves. *Antarctic Research Series*, **43**, 133-143.

MCWILLIAMS, J.C. 1977. A note on a consistent quasigeostrophic model in a multiply connected domain. *Dynamics of Atmosphere and Ocean*, **1**, 427-441.

POZDEYEV, V.S. & KURININ, R.G. 1987. Noviye danniye o morfologii ledovoy tolshi i reljefe podliodnogo lozha i morskogo dna v juzhnoy chasti basseina moriya Ueddella (Zapadnaya Antarctida). [New data on the morphology of the ice cover and relief of the subglacial bed and sea bottom in southern part of the Weddell Sea basin (West Antarctica)]. *Antarktika. Doklady Komissii*, **26**. 66-71.

ROBIN, G.DE Q. 1979. Formation, flow, and disintegration of ice shelves. *Journal of Glaciology*, **24**, 259-271.

ROBIN, G.DE Q., DOAKE, C.S.M., KOHNEN, H., CRABTREE, R.D. JORDAN, S.R. & MÖLLER, D. 1983. Regime of the Filchner-Ronne ice shelves, Antarctica. *Nature*, **302**, 582-586.

SCHEDUIKAT, M. & OLBERS, D.J. 1990. A one-dimensional mixed layer model beneath the Ross Ice Shelf with tidally induced vertical mixing. *Antarctic Science*, **2**, 29-42.

SCHLOSSER, P. 1986. Helium: a new tracer in Antarctic oceanography. *Nature*, **321**, 233-235.

SCHLOSSER, P., ROETHER, W. & ROHARDT, G. 1987. Helium-3 balance of the upper layers of the northwestern Weddell Sea. *Deep-Sea Research*, **34**, 365-377.

SCHLOSSER, P., BAYER, R., FOLDVIK, A., GAMMELSROD, T., ROHARDT, G. & MÜNNICH, K.O. 1990. Oxygen 18 and Helium as tracers of Ice Shelf Water and water/ice interaction in the Weddell Sea. *Journal of Geophysical Research*, **95** (C3), 3253-3263.

SVERDRUP, H.U. 1940. Hydrology, Section II: Discussion. *B.A.N.Z. Antarctic Research Expedition 1929-31, Reports-Series A, III*, Oceanography, Part 2, 88-126.